Energy spectra of quantum turbulence: Large-scale simulation and modeling

Narimasa Sasa,[1] Takuma Kano,[1] Masahiko Machida,[1] Victor S. L'vov,[2] Oleksii Rudenko,[3] and Makoto Tsubota[4]

[1]*CCSE, Japan Atomic Energy Agency and CREST(JST), 5-1-5 Kashiwanoha, Kashiwa, Chiba 277-8587, Japan*

[2]*Department of Chemical Physics, The Weizmann Institute of Science, Rehovot 76100, Israel*

[3]*Department of Applied Physics, Eindhoven University of Technology, Eindhoven NL-5600 MB, The Netherlands*

[4]*Department of Physics, Osaka City University, Sumiyoshi-ku, Osaka 558-8585, Japan*

In a 2048^3 simulation of quantum turbulence within the Gross-Pitaevskii equation, it is demonstrated that the large-scale motions have a classical Kolmogorov-1941 energy spectrum $E(k) \propto k^{-5/3}$, followed by an energy accumulation with $E(k) \simeq$ const at k about the reciprocal mean intervortex distance. This behavior was predicted by the L'vov-Nazarenko-Rudenko bottleneck model of gradual eddy-wave crossover [L'vov, Nazarenko, and Rudenko, J. Low Temp. Phys. **153**, 140 (2008)], further developed in the paper.

I. INTRODUCTION

Hydrodynamic turbulence (HT)[1]—loosely defined as a random behavior of fluids—remains the most important unsolved problem of classical physics, as was pointed out by Richard Feynman.

Quantum turbulence (QT)—a trademark of turbulence in superfluid ^{3}He, ^{4}He, and Bose-Einstein condensates of cold atomic vapors[2]—has added a new twist in turbulence research, shedding light on old problems from a new angle. QT consists of a tangle of quantized vortex lines with a fixed core radius a_0 and a finite (quantized) velocity circulation $\kappa = h/M$, where M is the proper atomic mass.[2] The superfluid has zero viscosity, and in the *zero-temperature limit*, which is the simplest for theoreticians and reachable for experimentalists,[3] the QT's Reynolds number Re is infinite. This brings (at least, the zero-temperature) QT to a desired prototype for better insight into classical HT turbulence.

The tangle of vortex lines in QT is characterized by a mean intervortex distance ℓ. For large-R-scale motions with $R \gg \ell$, the vortex tangles are better understood as bundles of nearly parallel vortex lines with mean curvature of about R^2. For large scales, the quantization of vortex lines can be neglected and QT can be considered as classical, in which the energy density in k space, $E(k)$, is given by the celebrated Kolmogorov 1941 (K41) law:[4]

$$E_{\text{K41}}(k) = C\,\varepsilon^{2/3}k^{-5/3},$$
$$E(\boldsymbol{r}) \equiv \langle |\boldsymbol{u}(\boldsymbol{r})|^2 \rangle/2 = \int E(k)\,dk, \tag{1}$$

confirmed experimentally and numerically.[1] Here, $C \sim 1$, ε is the energy flux over scales, and $E(\boldsymbol{r})$ is the energy density of turbulent velocity fluctuations per unit mass. Kelvin waves (KWs) are helix-like deformations of vortex lines with wavelength λ: $a_0 < \lambda < \ell$. Interactions of KWs on the same vortex line but with different $k \sim \lambda^{-1}$ lead to turbulent energy transfer toward large k. This idea (Svistunov[5]) was developed and confirmed theoretically and numerically by Vinen *et al.*,[6] Kozik and Svistunov (KS),[7] and L'vov and Nazarenko (LN).[8] Two versions of the KW spectrum were suggested in Refs. 7 and 8:

$$E_{\text{KS}}(k) = C_{\text{KS}}\Lambda\,\varepsilon^{1/5}\kappa^{7/5}\ell^{-8/5}k^{-7/5}, \text{ KS}, \tag{2a}$$

$$E_{\text{LN}}(k) = C_{\text{LN}}\Lambda\,\varepsilon^{1/3}\kappa\,\Psi^{-2/3}\ell^{-4/3}k^{-5/3}, \text{ LN}, $$
$$\Lambda \equiv \ln(\ell/a_0). \tag{2b}$$

Here, $C_{\text{KS}} \gg 1$, $C_{\text{LN}} \simeq 1/\pi$ (Ref. 9), and $\Psi < 1$ characterizes the ratio of ℓ to the large-scale modulation of the vortex lines. Parameter $\Lambda \simeq 12$–15 in typical experiments in ^{3}He and ^{4}He.[3] The choice between Eqs. (2) is under intensive debates,[10–13] which, however, has no principle effect on issues discussed in this paper.

The nature of the energy transfer and the energy spectrum is under intensive debate, too. Considering the inertial (Re$\rightarrow \infty$) energy transfer at the crossover scale $k \sim \ell^{-1}$, L'vov-Nazarenko-Rudenko (LNR) pointed out[14] that for $k \sim \ell^{-1}$ and $\Lambda \gg 1$ the KWs have much greater energy (2) than the HT energy (1) at the same energy flux ε. As a result, LNR predicted a bottleneck energy accumulation around $k \sim \ell^{-1}$. In contrast, KS suggested[15] an alternative scenario due to possible dominance of vortex reconnections in the energy transfer at $k \sim \ell^{-1}$ without any energy stagnation. In Ref. 16, LNR predicted two thermal-equilibrium regions between the HT (1) and KW (2) energy-flux spectra: with equipartition of the HT energy, $E(k) \propto k^2$, followed by equipartition of KW energy, $E(k) \simeq$ const.

Direct numerical simulations (DNS) of QT mostly use the Gross-Pitaevskii equation (GPE),[17] which in dimensionless form is given by

$$2\,i\partial\psi/\partial t + \nabla^2\psi = g|\psi|^2\psi. \tag{3}$$

The macroscopic wave function $\psi(\boldsymbol{r},t)$ plays the role of the complex order parameter, and g is the coupling constant. The transformation $\psi = \sqrt{\rho}\,e^{i\theta}$ maps Eq. (3) to the Euler equation for an ideal compressible fluid of density ρ and velocity $\boldsymbol{u} = \nabla\theta$ and an extra quantum pressure term.

The numerical study of QT by GPE Eq. (3) has been reported in a few papers so far. Nore *et al.*[18] solved the GPE with resolutions up to 512^3 and observed that, as the quantized vortices became tangled, the incompressible kinetic energy spectra seemed to obey the K41 law (1) for a short period of time but eventually deviated from it. Kobayashi and Tsubota[19] solved the GPE on a 256^3 grid with an extra dissipation term at small scales and showed the K41 law (1) more clearly. Yepez *et al.*[20] simulated the GPE on grids up to 5760^3 by using

a unitary quantum lattice gas algorithm. They also found a spectrum $E(k) \propto k^{-5/3}$ and interpreted it as the K41 law (1) of HT turbulence. However, due to the choice of initial conditions, their simulation should correspond to the pure KW region $k > \ell^{-1}$ [thus supporting the LN spectrum (2b) of KWs].

In the present paper, we solved the GPE on grids up to 2048^3 by parallelizing the simulation code on Earth Simulator (a vector-parallel machine).[21] In contrast to Ref. [20], we focused on HT and crossover regions, $k \lesssim \ell^{-1}$. First, we confirmed the K41 law (1) in an HT region of about two decades in length, which is wider than that of any previous work. Second, the visualization of vortices clearly shows the bundle-like structure, which has never been confirmed in GPE simulations on smaller grids. Third, we discovered a plateau in the crossover region, $k\ell \gtrsim 2\pi$, further explained as the KW's energy equipartition in the framework of the LNR's bottleneck model,[16] which is revised here to account for the recently predicted[8] and numerically observed[20] LN spectrum (2b) of KWs.

We consider this correspondence as a support in favor of LNR bottleneck theory, understanding, nevertheless, that interpretation of numerical (or experimental) data with the help of a theoretical model on the edge of its applicability (here $\Lambda \sim 1$) is often problematic, being a question of experience, physical intuition, and taste. Currently we cannot fully exclude the alternative KS scenario,[15] even though it gives no energy stagnation for $\Lambda \gg 1$. More theoretical studies and numerical and laboratory experiments are required to fully understand the vortex dynamics in the crossover region of scales.

II. NUMERICAL PROCEDURE AND RESULTS

In DNS, we follow procedure[19] but extend the maximum computational grid size from 256^3 up to 2048^3. The initial state is prepared by distributing random numbers created inside a range from $-N\pi\alpha$ to $N\pi\alpha$ into the phase $\theta(\mathbf{r})$ on selected points M^3 ($M \ll N$) and interpolating them to make a smooth velocity field on all grid points. Here, N is the total number of grid points and α is a control parameter for the initial energy input. Also, following Ref. [19], we add to the GPE an effective artificial energy damping for small-scale motions by replacing in the Fourier transform of the GPE $i \rightarrow i + 1$ for $k_x, k_y, k_z > 2\pi/\xi$, where $\xi \simeq a_0$ is the condensate coherence length.

GPE conserves the total number of particles and the total energy (Hamiltonian) of the system.[17] We decompose[18,22] the total energy density into the internal, $E_{\text{int}} \equiv g(\rho - 1)^2/4$, the quantum, $E_{\text{qnt}} \equiv |\nabla\sqrt{\rho}|^2/2$, and the kinetic, $E \equiv \rho|\mathbf{u}|^2/2$, energy densities. The kinetic energy is decomposed into compressible and incompressible components, both of which are monitored. Two typical spectra of the incompressible component are plotted in Fig. 1 with corresponding vortex distributions. The plot illustrates a 512^3 run at times 3.8 and 7.8 in the left and right panels, respectively (with the time being normalized by $2m\xi^2/\hbar$ and the distance by ξ). The time evolution of the equation is calculated by a symplectic integral method, and a typical pseudo-spectral method is employed for the calculation of the kinetic energy term. The method is a standard one, which is known to guarantee sufficiently high accuracy for hydrodynamics simulations. In Fig. 1 (left), one finds that the major part of the energy spectrum fits the K41 law (1), as in Ref. [19], but with a large inertial interval.

As expected, we also observed tangled vortex bundles, clearly demonstrated in the insets of Fig. 1, showing an x-y two-dimensional slice of the polarization field's color map, which is defined by summing vortices (± 1) inside plaquettes lying within a constant radius ($= 32\Delta x$) from a grid point. On the other hand, Fig. 1 is a typical example of a considerably decayed state, in which the main features are rather small vortex rings distributed almost equally inside the simulation cubic region.

An important observation (Fig. 1) is a plateau-like region for $k\xi \gtrsim 1.5$—a definite pileup over the K41 spectrum; this is a clear manifestation of the energy stagnation.

The main numerical result of the present paper is Fig. 2. The left panel shows an intercomparison of the incompressible kinetic energy spectrum $E(k)$ among 512^3, 1024^3, and 2048^3 simulations. The K41 scaling (1) (shown as cyan dash-dotted lines) is extended to the lower-k range with the grid-size increase. This is the first clear demonstration of the classical K41 scaling characteristic for the normal-fluid turbulence but maintained in the large-scale range of the superfluid turbulence. The visible extent of the K41 scaling on the 2048^3 grid is much larger than that in all previous simulations.

The right panel of Fig. 2 displays self-similar large structures of tangled vortices in the fully turbulent state: the large-scale vortex bundles in the maximum size, 2048^3, and
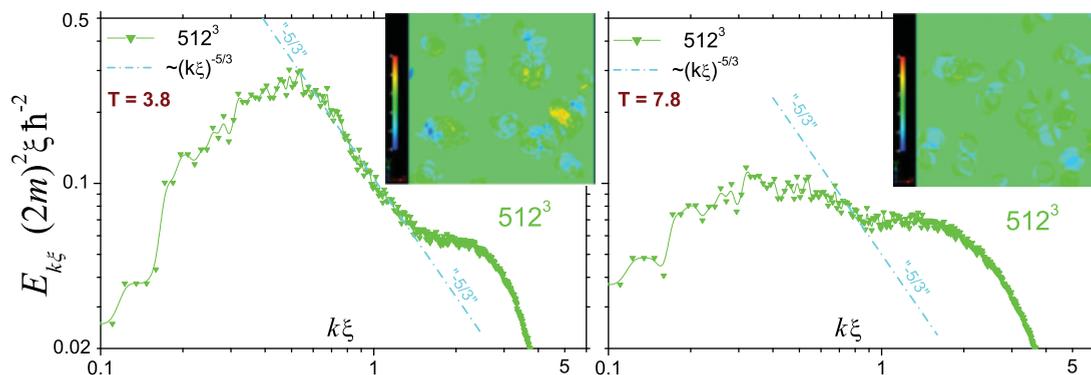
FIG. 1. (Color online) The incompressible energy spectra at time $T = 3.8$ (left) and $T = 7.8$ (right). The color insets show vorticity two-dimensional slice maps (see text for the definition). The grid size is 512^3 and $\Lambda \simeq 1.5$.
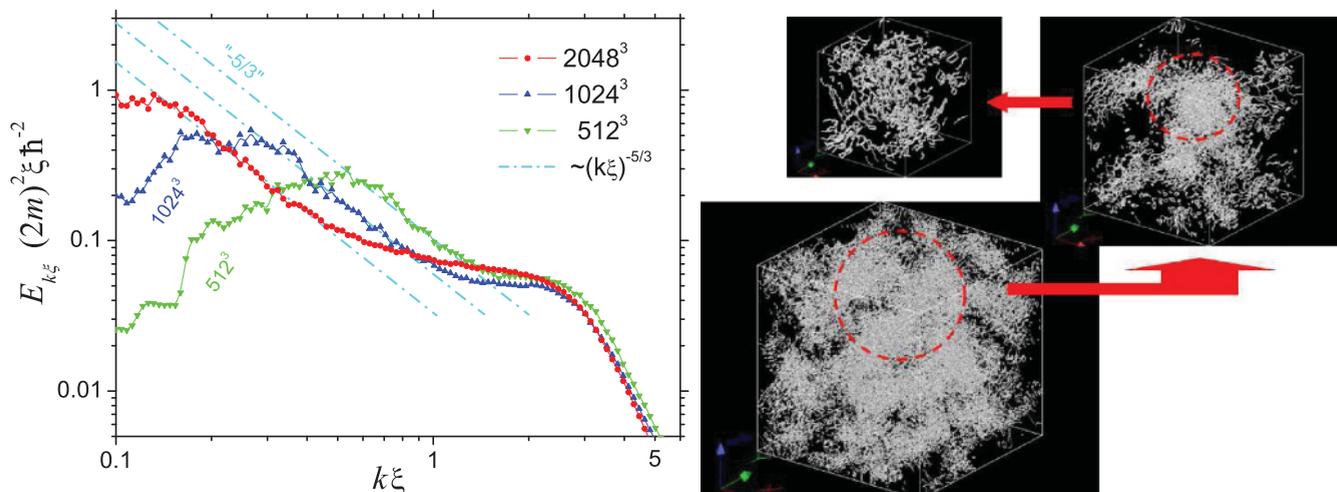
FIG. 2. (Color online) Left: Simulation results of the incompressible energy spectra $E(k\xi)$ normalized by $\hbar^2/(4m^2\xi)$. Symbols: 2048^3 ($-\bullet-$), 1024^3 ($-\blacktriangle-$), 512^3 ($-\blacktriangledown-$). Λ varies from $\Lambda \simeq 1.5$ (slightly depending on time) for 512^3 to $\Lambda \simeq 2.2$ for 2048^3. Dot-dashed (cyan) line: K41 "−5/3" scaling. Right: A snapshot of vortex lines at the fully developed turbulent state of 2048^3 demonstrates the self-similarity of the bundle-vortex structure (see the dotted circles representing the zoomed regions whose vortex distributions are shown subsequently), typical for fully developed turbulence.

smaller self-similar tangled structures inside this cubic region in the subsequent insets.

Before discussion of these results, we will revise shortly in the next section the LNR model of the bottleneck crossover[16] to account for the recently predicted LN spectrum of KWs.[8]

III. LNR MODEL OF THE BOTTLENECK CROSSOVER

To find theoretically $E(k)$, we, following LNR,[16] approximate the superfluid motions as a mixture of "pure" HT and KW motions with the spectra $E^{\mathrm{HT}}(k) \equiv g(k\ell)E(k)$ and $E^{\mathrm{KW}}(k) \equiv [1 - g(k\ell)]E(k)$. Here, $g(k\ell)$ is the "blending" function, which was found in Ref. 16 by calculation of energies of correlated and uncorrelated motions produced by a system of ℓ-spaced wavy vortex lines:

$$g(x) = g_0[0.32 \ln(\Lambda + 7.5)x],$$
$$g_0(x) = \left[1 + \frac{x^2 \exp(x)}{4\pi(1 + x)}\right]^{-1}.$$

The total energy flux ε_k, also consisting of HT and KW contributions,[16] is modeled by dimensional reasoning in the differential approximation. Hence, for $k \to 0$ the energy flux is purely HT and thus $\varepsilon_k \propto k^{-2}\sqrt{E^{\mathrm{HT}}}dE^{\mathrm{HT}}/dk$. From the other side, for $k \to \infty$ the energy flux is purely KW and thus $\varepsilon_k \propto [E^{\mathrm{KW}}]^2 dE^{\mathrm{KW}}/dk$. Importantly, in contrast to Ref. 16, where the physically irrelevant KS spectrum of KWs (2a) was used, we employ here the proper LN spectrum (2b) that accounts for large-scale vortex-line modulations with short KWs.[8] The full equation for the total energy flux reads

$$-\left\{\frac{1}{8}\sqrt{k^{11}g(k\ell)E(k)} + \frac{3}{5}\frac{\{\Psi k^3 k_* \ell^2[1 - g(k\ell)]E(k)\}^2}{(C_{\mathrm{LN}}\Lambda\kappa)^3}\right\}$$
$$\times \frac{d}{dk}\left\{E(k)\left[\frac{g(k\ell)}{k^2} + \frac{1 - g(k\ell)}{k_*^2}\right]\right\} = \varepsilon_k. \quad (4)$$

Here, $E^{\mathrm{HT}}(k_*) = E^{\mathrm{KW}}(k_*) \Rightarrow k_*\ell \simeq 6.64/\ln(\Lambda + 7.5)$. In the inertial range, the energy flux is constant, $\varepsilon(k) = \varepsilon$. Moreover, in the system of quantum filaments it is related to the root-mean-square vorticity $\sqrt{\langle|\boldsymbol{\omega}|^2\rangle} \simeq \kappa/\ell^2$ via $\langle|\boldsymbol{\omega}|^2\rangle = 2\int k^2 E(k)dk$ (see Refs. 1 and 2). This allows us to find solutions of Eq. (4) for different Λ, as depicted in Fig. 3 by black dashed and solid curves. (For the sake of better comparison we replotted the simulation data, bringing them all together to the LNR model curve with $\Lambda = 2$ by superposing the K41 and plateau regions. This is achieved by fitting the mean intervortex distance ℓ, which is greed-size dependent:
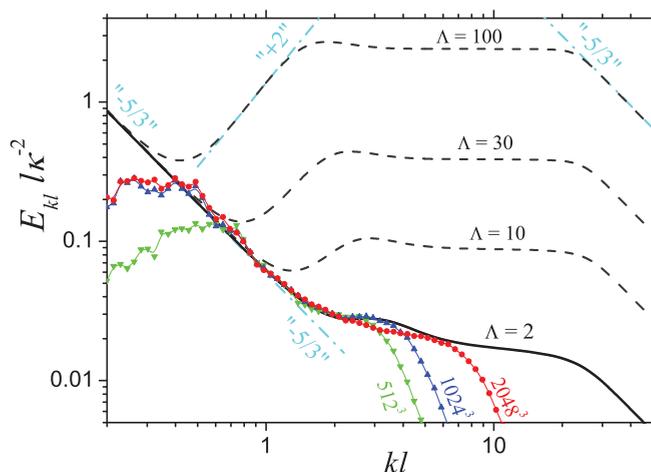
FIG. 3. (Color online) Incompressible energy spectra plotted vs $k\ell$ and normalized by κ^2/ℓ. The simulation results (the same symbols) and the LNR model for $\Lambda = 10, 30, 100$ [dashed (black) curves] are brought together to the theoretical [solid (black)] curve with $\Lambda = 2$ by superposing the K41 (for both simulations and model) and plateau regions (only for simulations). Dot-dashed (cyan) lines show different scaling asymptotics.

the computation of ℓ is approved *a posteriori* only if $\ell \gg a_0$; in our case, $\Lambda \sim 1$, ℓ may be considered as a fitting parameter.)

Four distinct scaling regions are evident ($\Lambda \gg 1$):

(a) $k\ell \ll 1$: $E(k)$ and ε_k are dominated by the pure HT contributions, and the K41 law (1) is revealed.

(b) $k\ell \gg 1$: $E(k)$ and ε_k are dominated by the pure KW contributions, and one observes the LN spectrum (2b) of KWs with a constant energy flux.

(c) $k \lesssim k_*$: As explained above, for $\Lambda \gg 1$ the KW turbulence is much less efficient in the energy transfer over scales than its HT counterpart with the same energy, which leads to the (HT) energy accumulation with a level $E(k) \approx E^{\text{HT}}(k) \gg E_{\text{K41}}(k)$. For $k \lesssim k_*$, both $E(k)$ and ε_k are still dominated by HT contributions, but the energy flux is much smaller than the K41 estimate requires. This is like a flux-free HT system; thus, thermodynamic equilibrium is expected with the equipartition of energy between the degrees of freedom: the three-dimensional energy spectrum is constant; hence, the one-dimensional energy spectrum $E^{\text{HT}}(k) \propto k^2$. This scaling is observed in Fig. 3, for $k \lesssim k_*$. Think of a pond before a dam, where the water velocity, being much smaller than that in the source river, does not affect the water level, which is practically horizontal. This interpretation of the energy bottleneck effect as "incomplete thermalization" (of only the high-k region) was suggested by Frisch *et al.*[23]

(d) $k \gtrsim k_*$: Unexpectedly, we observe here almost a k-independent one-dimensional energy spectrum, $E(k) \approx \text{const}$, inherent to the thermodynamic equilibrium of KWs. In the pure KW system, such a spectrum shows up for $k \gg k_*$. However, in region 4, the energy of the system is already dominated by the KW contributions, $E(k) \approx E^{\text{KW}}(k)$, while the energy flux is still dominated by the HT motions.[16] Hence, this is almost a flux-free system of KWs, which is indeed found in thermodynamic equilibrium with the one-dimensional energy equipartition, $E(k)^{\text{KW}} = \text{const}$.

As one sees from Fig. 3, with the decrease of Λ the pileup becomes less pronounced. For $\Lambda = 2$, the equilibrium HT region (3) almost disappeared; however, the equilibrium KW region (4) is still well pronounced, being much less sensitive to the value of Λ.

IV. DISCUSSION AND SUMMARY

A. Classical and quantum energy bottleneck effects

The bottleneck effect in classical HT is understood traditionally[24,25] as a hump on a plot of compensated energy spectrum $E(k)k^{5/3}$ in the crossover region between inertial and viscous intervals. This is a very general phenomenon, reported in many numerical simulations and experiments of classical hydrodynamic turbulence. For example, Yeung and Zhou,[26] Gotoh *et al.*,[27] Kaneda *et al.*,[28] and Dobler *et al.*[29] found the bottleneck effect in their numerical simulations. Saddoughi and Veeravalli[30] studied the energy spectrum of atmospheric turbulence and reported the bottleneck effect. Shen and Warhaft,[31] Pak *et al.*,[32] She and Jackson,[33] and other experimental groups also observed the bottleneck effect in fluid turbulence. The bottleneck effect has been seen in other forms of turbulence as well (see, e.g., Refs. 11–16 in Ref. 24).

To characterize the value of this effect, one can introduce a "bottleneck magnitude" M_{bn}: the hump height, normalized by the plateau value of $E(k)k^{5/3}$ in the inertial interval. For example, in high-resolution DNS of the classical HT,[24] shown in Fig. 4 (left), its magnitude $M_{\text{bn}} \simeq 0.34$ for 512^3 DNS and decreases with an increase in resolution: $M_{\text{bn}} \simeq 0.31$ for 1024^3 and $M_{\text{bn}} \simeq 0.25$ for 2048^3. Recent results[25] based on the 4096^3 DNS confirm the statement that the bottleneck magnitude in classical turbulence systematically decreases with increasing DNS resolution (or, equivalently, with the Taylor-Reynolds number Re_λ growth, and $M_{\text{bn}} \to \text{Re}_\lambda^{-0.4}$ as $\text{Re}_\lambda \to \infty$).

Coming to a comparison of the bottleneck effects in our modeling and numerical simulations, we should note that the LNR model accounts only for leading order in $\Lambda = \ln(\ell/a_0)$ terms.[14,16] Moreover, it is based on the differential approximation for the energy flux, which is reasonable for vivid power-like behavior of the energy spectra, which exists
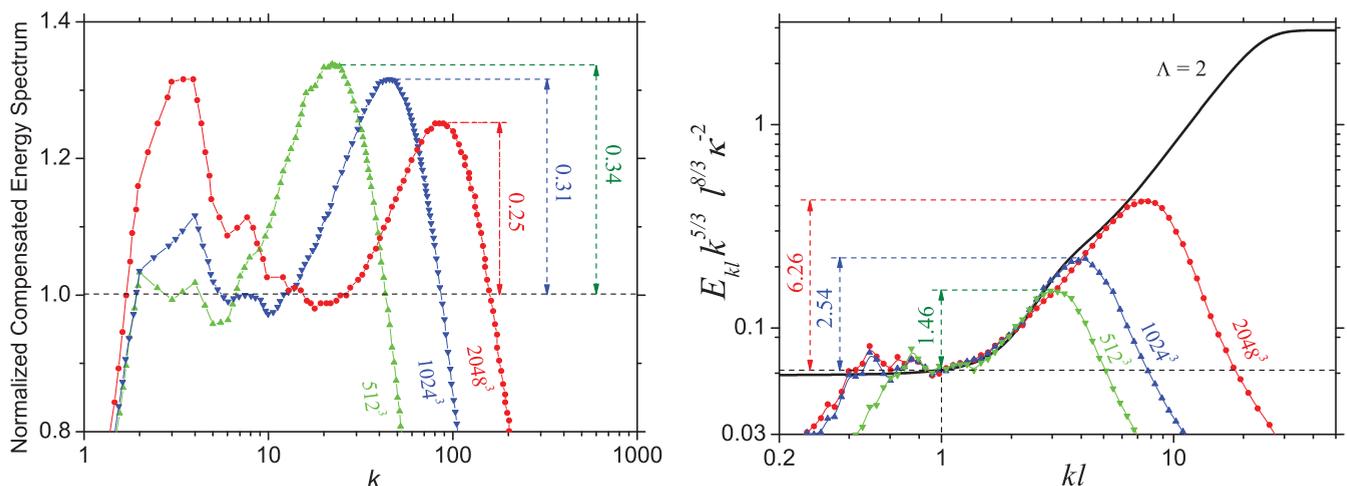
FIG. 4. (Color online) Comparison of the compensated energy spectra $E(k)k^{5/3}$ (using the same color-symbol code as in previous figures) and of the bottleneck magnitudes M_{bn} (dashed color arrows). Left: DNS data of classical HT[24] (cf. Fig. 1 in Ref. 24): modest values of $M_{\text{bn}} \lesssim 1.34$ decrease with the increase of the resolution. Right: Our DNS data of quantum superfluid turbulence: large values of M_{bn} increase with the resolution up to $M_{\text{bn}} \simeq 6.26$.

only for $\Lambda \gg 1$ (Fig. 3). Therefore, one expects that the LNR model is suitable for quantitative analysis of experiments in ^{3}He and ^{4}He, where $\Lambda \simeq 12$–15, and can only qualitatively describe the simulations presented here with $\Lambda \simeq 2$.

Nevertheless, the simulations clearly demonstrate in Fig. 3 the plateau that immediately follows the K41 scaling (1), which agrees with the LNR model prediction for $\Lambda \simeq 2$ (Fig. 3). The plateau broadens with the grid-size increase toward that of the LNR model curve (with the earlier cutoff of the simulation data being due to the artificial dissipation). The resolution of the current simulations does not allow us to resolve the KW scaling (2b) with constant energy flux, as was done in Ref. 20, but the bottleneck is definitely there.

To measure bottleneck magnitudes in QT, we replotted our data from Fig. 3, compensating $E(k)$ by the K41 prediction, i.e., multiplying by $(k\ell)^{5/3}$ (see Fig. 4, right). One sees large humps with magnitudes $M_{\rm bn}$ that increase with the resolution, reaching $M_{\rm bn} \simeq 6.26$ for 2048^3. Recall that in classical turbulence $M_{\rm bn}$ is much smaller (by an approximate factor of 20) and demonstrates the opposite tendency with the resolution.

We concluded that classical and quantum bottlenecks have completely different natures. The small magnitude of the bottleneck in classical turbulence is related to some nonlocality of the energy transfer toward small scales, which is slightly suppressed due to the fast decrease of the turbulence energy in the dissipation range, while in QT (at zero temperature) the essential bottleneck effect originates from the strong suppression of the energy flux in the KW region.

Indeed, Fig. 4 (right) demonstrates the good agreement between the QT DNS data and the LNR model prediction (which accounts for the flux suppression mentioned above) for $\Lambda \simeq 2$, which improves by increasing the DNS resolution. The cutoff of the spectra for large k is a consequence of limited k space in the simulations. We predict that with the further increase of the resolution the bottleneck magnitude can reach $M_{\rm bn} \simeq 50$ at $\Lambda \simeq 2$ and even much larger values for larger Λ.

B. Summary

In this paper, we conclude that the observed essential bottleneck energy accumulation has a definite quantum nature (quantization of circulation) and can be completely rationalized within the LNR model of gradual eddy-wave crossover, suggested in Ref. 16. We consider this model as a minimal model of QT that describes homogeneous isotropic turbulence in superfluids with energy pumped at scales much larger than the mean intervortex distance and reveals reasonable (and even unexpectedly good) agreement with the simulations of the GPE discussed here. The reason is that in the most questionable crossover region the LNR model predicts a local thermodynamic equilibrium, where the energy spectra are universal and insensitive to the details of microscopic mechanisms of interactions (e.g., vortex reconnections).

[1] U. Frisch, *Turbulence* (Cambridge University Press, Cambridge, 1995).

[2] W. F. Vinen and R. J. Donnelly, Phys. Today **60**(4), 43 (2007); M. Tsubota, J. Phys. Soc. Jpn. **77**, 111006 (2008).

[3] V. B. Eltsov, R. de Graaf, R. Hanninen, M. Krusius, R. E. Solntsev, V. S. L'vov, A. I. Golov, and P. M. Walmsley, in *Progress in Low Temperature Physics: Quantum Turbulence*, Vol. 16, Chap. 2 (Elsevier, 2009), pp. 45–146.

[4] A. N. Kolmogorov, Dokl. Akad. Nauk SSSR **30**, 9 (1941); **32**, 19 (1941); Proc. R. Soc. Ser. A **434**, 9 (1991); **434**, 15 (1991).

[5] B. V. Svistunov, Phys. Rev. B **52**, 3647 (1995).

[6] W. F. Vinen, M. Tsubota, and A. Mitani, Phys. Rev. Lett. **91**, 135301 (2003).

[7] E. Kozik and B. V. Svistunov, Phys. Rev. Lett. **92**, 035301 (2004); **94**, 025301 (2005); Phys. Rev. B **72**, 172505 (2005).

[8] V. S. L'vov and S. Nazarenko, Pisma v ZhETF **91**, 464 (2010).

[9] L. Boue, R. Dasgupta, J. Laurie, V. S. L'vov, S. Nazarenko, and I. Procaccia, e-print arXiv:1103.5967.

[10] J. Laurie, V. S. L'vov, S. Nazarenko, and O. Rudenko, Phys. Rev. B **81**, 104526 (2010).

[11] V. V. Lebedev and V. S. L'vov, J. Low Temp. Phys. **161**, 548 (2010).

[12] V. V. Lebedev, V. S. L'vov, and S. V. Nazarenko, J. Low Temp. Phys. **161**, 606 (2010).

[13] E. Kozik and B. V. Svistunov, Phys. Rev. B **82**, 140510(R) (2010).

[14] V. S. L'vov, S. V. Nazarenko, and O. Rudenko, Phys. Rev. B **76**, 024520 (2007).

[15] E. Kozik and B. V. Svistunov, Phys. Rev. B **77**, 060502 (2008); Phys. Rev. Lett. **100**, 195302 (2008).

[16] V. S. L'vov, S. V. Nazarenko, and O. Rudenko, J. Low Temp. Phys. **153**, 140 (2008).

[17] L. Pitaevskii and S. Stringari, *Bose-Einstein Condensation* (Oxford University Press, New York, 2003).

[18] C. Nore, M. Abid, and M. E. Brachet, Phys. Rev. Lett. **78**, 3896 (1997); Phys. Fluids **9**, 2644 (1997).

[19] M. Kobayashi and M. Tsubota, Phys. Rev. Lett. **94**, 065302 (2005); J. Phys. Soc. Jpn. **74**, 3248 (2005).

[20] J. Yepez, G. Vahala, L. Vahala, and M. Soe, Phys. Rev. Lett. **103**, 084501 (2009).

[21] The Earth Simulator Center [http://www.jamstec.go.jp/esc/index.en.html].

[22] R. Numasato, M. Tsubota, and V. S. L'vov, Phys. Rev. A **81**, 063630 (2010).

[23] U. Frisch *et al.*, Phys. Rev. Lett. **101**, 144501 (2008).

[24] M. K. Verma and D. Donzis, J. Phys. A **40**, 4401 (2007).

[25] D. Donzis and K. R. Sreenivassan, J. Fluid Mech. **657**, 171 (2010).

[26] P. K. Yeung and Y. Zhou, Phys. Rev. E **56**, 1746 (1997).

[27]T. Gotoh, D. Fukayama, and T. Nakano, Phys. Fluids **14**, 1065 (2002).

[28]Y. Kaneda, T. Ishihara, M. Yokokawa, K. Itakura, and A. Uno, Phys. Fluids **15**, L21 (2003).

[29]W. Dobler, N. E. L. Haugen, T. A. Yousef, and A. Brandenburg, Phys. Rev. E **68**, 26304 (2003).

[30]S. G. Saddoughi and S. V. Veeravalli, J. Fluid Mech. **268**, 333 (1994).

[31]X. Shen and Z. Warhaft, Phys. Fluids **12**, 2976 (2000).

[32]H. K. Pak, W. I. Goldburg, and A. Sirivat, Fluid Dyn. Res. **8**, 19 (1991).

[33]Z. S. She and E. Jackson, Phys. Fluids A **5**, 1526 (1993).